Reconstructing the Visual Field of Compound Eyes

Steven Collins

Image Synthesis Group, Trinity College Dublin

Abstract:
Realistic image synthesis research involves the simulation of visible light propagation within an environment with a view to computing an image that evokes a similar visual response to that perceived by an observer of that environment. This has involved the use of both sophisticated camera response and human visual system response models. In this paper we investigate the application of invertebrate vision models, in particular the vision from compound eyes. We use *Apis meliferra* (or honey bee) as a case study, constructing a geometric model of the retinal structure of the eye and applying psychophysical data obtained from physiological, morphological and behavioural studies regarding spectral sensitivity and spatial acuity in order to reconstruct an image approximating that perceived by a bee. The algorithm is general and can be adapted to other invertebrate families.

Keywords: realistic image synthesis, vision, perception, compound eye.

1 Introduction

Research into global illumination and realistic image synthesis has, hitherto, concentrated on the computation of an image from the point of view of either a camera system or a human visual observer. The camera models employed have ranged from the computationally convenient but non-physically based pinhole camera model to more sophisticated treatments of lens assemblies, accounting for non-linearity in the sensor radiometric sensitivity and depth of field and vignette artifacts [PC81][CPC84][KMH95]. The final result is a mapping from the irradiance of the sensor to an appropriate choice of RGB tuple for display. More recently, new models [War94][TR93] have employed psychophysical data regarding the response of a human observer system to visual stimuli of varying spectral and radiometric distributions. These models employ *tone reproduction operators* which attempt to preserve brightess and contrast features when mapping the irradiance field to the required display. Meyer [MG88] proposes a colour model which accounts for different forms of colour blindness and attempts to visualise the appearance of an scene as viewed by a colour-blind person. Nakame et al. [NKON90] introduce a model of glare and diffraction to simulate the visual conditions when driving under varying conditions. To further improve the appearance of brightness on devices with limited luminance bandwidth, Spencer et al. [SSZG95] introduce a model of *glare* which reproduces the human eye's scattering and diffraction behaviour under various lighting conditions. More recently a model of visual adaptation [FPSG96] has been proposed which models the change in spectral sensitivity and spatial acuity due to varying environmental luminance levels.

This model accounts for the shift between *scotopic*, *mesopic* and *photopic* modes of visual perception and also temporal changes in visual sensitivity due to sudden changes in luminance levels.

In addition to the quest for visual realism, psychophysical data of this nature may be employed to guide the global illumination algorithm itself, directing effort in directions or wavelength bands where it will be most perceived. Meyer [Mey88] proposed a colour space and spectral sampling strategy based on the human spectral sensitivity functions which minimises the spectral sampling density. Bolin et al. [BM95] employ data regarding the spatial and spectral acuity of the visual system to guide image sampling strategies, adapting to edges and minimised sample density in regions of low radiance gradient.

1.1 Non-human Visual Response

If psychophysical and optics geometry information is available then it is possible to reconstruct the vision of any animal. The optics of the animal, including cellular distribution, field of view and optic transfer mechanisms may be used to govern a global illumination sampling strategy. The resulting radiance distributions are then modulated by the animal's spectral and spatial sensitivities to produce *response functions* making up the final image. For display, however, these functions must be mapped to monitor illuminances which are perceived by a human observer. How, therefore, is it possible to "see" what the animal sees. For example, the honey bee is highly sensitive to ultra-violet (UV) light energy. We would compute an image which has high response levels to UV, but for display purposes, this response must be mapped to the monitor gamut and finally viewed. While it may be quite feasible to manufacture a display device with an appropriate gamut (including UV), this would be of little use, visually, to the human observer. Thus, the choice of mapping bee response to monitor gamut is arbitrary, and different mappings may be employed to highlight various aspects of the animal's visual system. Thus, this mapping is a *visualisation phase* rather than a display of absolute animal visual perceptual quantities.

1.2 Vision of *Apis mellifera*

We choose to study *Apis mellifera* or honey bee which has one of the more sophisticated vision systems of the *hymenoptera* family of invertebrates and which has seen most research devoted to it. The bee is equipped with 2 side-facing compound eyes composed of a hexagonal array of between 4700 and 10000 facets[1]. The distribution of facet size varies across the surface of the eye and from one bee class to another. Bees, due to the wide field of view and opposing directions of their eyes do not employ stereopsis, relying on luminance edge detection and parallax for distance estimation.

Bees, like many other hymenoptera, are highly sensitive to UV light which dominates their visual perceptual responses. Remarkably, they possess a trichromatic opponent colour processing system [RM80][Hel92] similar to that of humans, but with peak spectral sensitivites at $\lambda_{UV} = 350nm$, $\lambda_{blue} = 440nm$ and $\lambda_{green} = 530nm$. Bees, like most insects, have little or no sensitivity in the longer wavelength regions.

[1] Worker bees[PRWW80] have 4752 ± 35 facets whereas drone bees 9973 ± 56 facets.

For navigation, in addition to being sensitive to the magnetic field of the earth, bees are capable of perceiving the direction of light polarization[Fri67]. This sensitivity is due to morphological aspects of the retinal cell which we will discuss in Section 2. It is generally regarded, however, that polarization sensitivity does not manifest itself as a modulation of the perceived brightness but rather is processed as a separate quantity in the retinal cell.

Although we are interested in the visual response of the animal, it is interesting to note that polarization processing occurs in receptors which are highly UV sensitive and optomotor responses[2] are tied to green receptors.

2 Functional Geometry and Morphology of the Compound Eye

Each receptor of the compound eye is composed of an ommatidium structure at the centre of which is the *rhadbom* which houses the photosensitive cells and an optical system which focusses incoming light onto the rhabdom tips. The relationship between these subsystems gives rise to a classification (see Figure 1) of the compound eye by Exner (1981):

apposition eyes: light entering the optical system of one receptor reaches only those cells in the associated rhabdom of that receptor.

superposition eyes: light from neighbouring optical systems contribute to the total light flux reaching a given rhabdom.

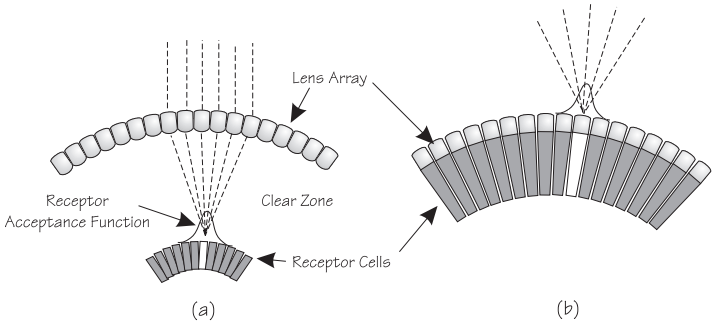

Fig. 1. Image formation by compound eyes. (a) is a clear-zone superposition eye with neighbouring corneal lenses contributing to the illumination on a given rhabdom. (b) is an apposition eye, with a one-to-one relationship between lens and rhabdom.

True superposition eyes are relatively rare (the Hesperiidae butterfly being a good example) and are usually associated with a *clear-zone* optical system (i.e. a layer of lens cells and a layer of rhabdomeres separated by a wide clear region). The bee eye is a good example of an apposition eye. Each rhabdom has its

[2] Optomotor responses are those which trigger motion of the animal for predator avoidance or target acquisition.

own distinct *dioptic system* composed of a *corneal lens* and a *crystalline cone*. This pair of elements directs the incoming light onto the tip of the rhabdom which carries the light through the length of the ommatidium via total internal reflection (the refractive index of the rhabdomeres is greater than that of the surrounding medium).

Facet shape varies according to the packing density of the ommatidia on the surface of the eye. In animals with a small number of receptors, the individual facets are approximately circular. The bee has a high density which gives rise to the area minimising hexagonal shape. The distribution of ommatidia size on the eye surface varies between bee classes [PRWW80]. The average facet diameter (see Figure 2), for the worker bee, is a maximum $17.7\mu m$ in the lower frontal region (used to fixate the hive entrance when entering) and ranges to $15\mu m$ in the dorsal (top facing) facets. The drone, on the other hand, has the largest facets (diameter $31\mu m$) both in the lower front but also in the upper frontal region (used to fixate the queen in-flight).

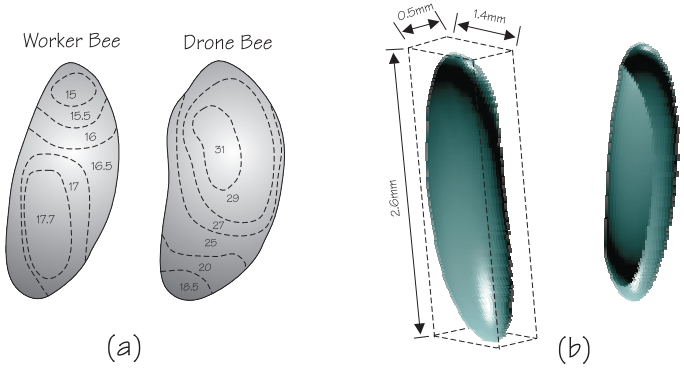

Fig. 2. Geometry of the bee compound eye. (a) based on von Praagh, depicts the distribution of facet diameter on the eyes of a drone and worker bee (all sizes given in mm). (b) shows the overall geometry of the eye pair.

The inter-ommatidial angle (between the central axes of neighbouring ommatidia) varies little over the entire surface of the eye [Lan90], ranging from approximately 1.5^o to 2.1^o.

2.1 The Ommatidium

The ommatidium is the functional component of the compound eye. It is a long tubular structure composed of a dioptic lens array connected to a twisted array of eight long visual cells and a ninth short visual cell. These are connected at the axis where the microvilli (the light sensitive fibres which appear like a comb along the length of each visual cell) join to form the rhabdom. The entire structure twists through a total of 180^o along its length.

The nine cells are classified [Gri75][MB76] according to function and spectral sensitivity (with numbers of each cell in each ommatidium given in brackets):

Type I: (2) UV sensitive and represent the largest of the visual cells, they extend the entire length of the ommatidium, $250 - 300\mu m$.

Type II: (4) Blue and green sensitive, extend the entire length of the ommatidium, $250 - 300\mu m$.

Type III: (2) Green sensitive, extend as far as the distal end of the ninth cell, $150 - 200\mu m$.

Ninth Cell (1) Existence only verified in 1972 [Gri75], it is only approx. $100\mu m$ long and is located at the proximal end of the ommatidium. There are no pigment cells in this cell.

Figure 3 depicts the ommatidium as a 3D model with a number of sections taken at intervals along the length demonstrating the change in layout. Note that the sections have not been rotated in line with the overall structure. Each of the cells direct light energy along its length in a manner similar to an optical fibre. Indeed studies of the ommatidium reveal that it acts approximately as an *cylindrical waveguide* transferring energy along its length as dielectric waveguide modes.

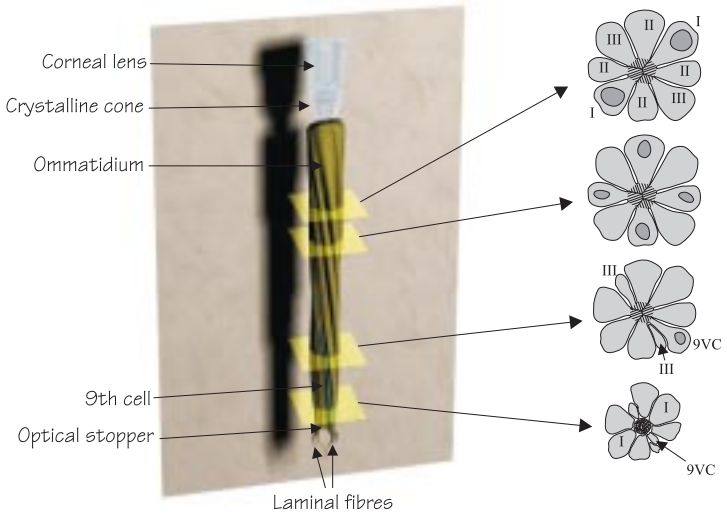

Fig. 3. On the left is a 3D model of the ommatidium structure. The dioptric apparatus of the receptor is composed of the corneal lens and cystalline cone. The relative position of the 9th visual cell is highlighted. The base of the structure is capped with opaque material to prevent light escaping. The laminal fibres transmit the electrical impulses from visual cells to lower cortex layers. On the right are 4 cross-sections adapted from Gribakin with cell classifications indicated.

The microvilli along the inner length of each rhabdom contain the *rhodopsin*[3]

[3] Rhodopsin pigments are also found in the cone cells of the human retina.

pigments that give rise to colour sensitivity. These microvilli are coherently oriented in four directions and undergo *dichroic absorption* where parallel and perpendicular components of the incident light waves are anisotropically absorbed. It is this arrangement that allows for polarization sensitivity, and although the cells twist through 180^o, thus eliminating their ability to uniquely determine polarization direction the shorter ninth cell still retains that capability.

3 A Model of Bee Visual Response

In order to compute an image representing the visual response of *Apis meliferra* we need both a camera model which captures the geometric structure of the compound eye and a bee tone mapping model to allow mapping of radiance values to bee-luminance quantities. The camera model is derived from the facet distribution and the angular acceptance function of the individual facets.

3.1 Visual Acuity

The visual resolving power may be defined as the capacity of a visual system to unambiguously transfer a patterned set of stimuli on the receptor layer. For a given compound eye this is a function of both the angular sensitivity of the individual ommatidia and the divergence angle, $\Delta\varphi$, between the axes of neighbouring ommatidia [Sny76][Weh75]. Sampling theory dictates that the highest spatial frequency resolvable will be

$$f_{max} = \frac{1}{2\Delta\varphi}$$

In general, however, this limit is never reached as the angular sensitivity of the receptors has a range greater than the inter-ommatidial angles. Angular sensitivity, $A(\theta)$ is defined by $\Delta\rho$, the half-width of the acceptance function at 50% sensitivity. $A(\theta)$ is determined by convolution of the *lens-pupil intensity function* and the *rhabdom acceptance function*[4]. Larger values of $\Delta\rho$ reduce contrast transfer as the visual fields of neighbouring receptors will overlap to a greater extent. Smaller valued of $\Delta\rho$ reduce total incident flux thus reducing overall sensitivity. $A(\theta)$ is approximately Gaussian[Sny76]:

$$A(\theta) \approx e^{-2.77\frac{2\theta}{\Delta\rho}}$$

where $A(\theta)$ is normalised to unity at maximum.

Thus there is a tradeoff. Indeed, the design of the entire compound eye is a design compromise: higher spatial acuity requires increased receptor density, leading to smaller receptor diameters which results in poorer sensitivity. In order for a compound eye to have similar resolution to that of the human eye, it would need to be approximately $12m$ in diameter.

[4] The lens-pupil intensity function is governed by the diffraction limited characteristics of the dioptic apparatus and the rhabdom acceptance function is derived from the flux loss due to absorption and wave-guide behaviour.

The *Rayleigh criterion*[5] states that 2 point sources will be resolvable if their angular separation exceeds

$$1.22\frac{\lambda}{D} \text{ radians}$$

where D is the diameter of the lens system and λ the wavelength of light. For a bee with $D = 25\mu m$ with $\lambda = 500nm$ this gives a resolution limit of 1.4^o [Lan90]. This agrees well with the actual values for $\Delta\varphi$ which ranges from 1.5^o to 3.1^o and $\Delta\rho$ which ranges from 2.5^o to 2.7^o.

3.2 Spectral Sensitivity

Spectral sensitivity of *Apis meliferra* is dependent on the luminance levels of the surrounding environment in a manner similar to the *scotopic* and *photopic* modes of human vision [RM80][MB76]. As with the human eye, the bee has an achromatic luminance threshold below which no illumination is registered. Within a range of low luminance levels, the bee's visual response is achromatic until the chromatic threshold is reached at which point spectral sensitivity is activated. Beyond a certain luminance level the bee reverts to achromatic vision. This process of adaptation is shown in Figure 4.

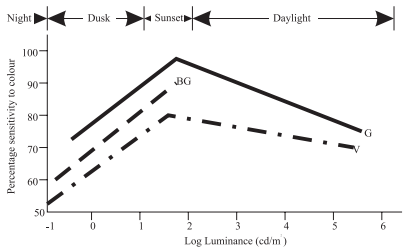

Fig. 4. Spectral sensitivity under varying lighting conditions (after Rose). For environment lighting levels ranging from night to daylight the percentage of correct choices of *Apis meliferra* for three colours, green (G), blue-green (BG) and violet (V) is shown. 50% represents complete lack of spectral sensitivity (either of 2 colours were chosen uniformly) whereas 100% means the bee chose the correct colour all the time.

As can be seen, below $\log 10^{-1} cd/m^2$ the bee responds achromatically. Between $\log 10^1$ and $\log 10^2$ sensitivity is at a maximum. Above luminance levels of $\log 10^2$ spectral sensitivity slowly decreases. Note that all colours exhibit similar curves indicating that there are no discernible *Purkinje shifts*[6]. Unfortunately,

[5] The Rayleigh criterion assumes that 2 point sources, viewed through a diffraction limited system (where the diameter of the aperature is small) can be separated when viewed if the image of one falls on the minimum of the *Airy disc* pattern due to the other.

[6] The Purkinje effect is the perceived hue shift due to a change from photopic to scotopic visual processing modes due to a shift in the luminous efficacy curves of the eye.

the data regarding bee light-dark adaptation is too sparse to permit useful simulation, being based on the results from 3 wavelengths alone.

The behavioural studies of von Helversen [Hel92] have yielded a spectral sensitivity function of the light-adapted bee, $S(\lambda)$, shown in Figure 3.2(a), which exhibits 3 peaks sensitivities at $345nm$, $440nm$ and $550nm$, where the sensitivities have relative proportions of $16 : 2.7 : 1$. This suggests a colour space with primaries of UV, B and G (ultraviolet, blue and green respectively). Rose et al. proposed such a colour space [RM80] which is functionally similar to the CIExy chromaticity diagram. This is shown in Figure 5(b).

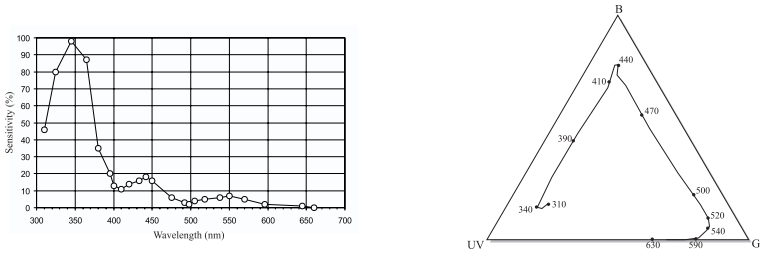

(a) (b)

Fig. 5. (a) Spectral sensitivity of *Apis meliferra* showing peak sensitivities at $345nm$, $440nm$ and $550nm$ (after von Helversen). (b) The bee colour triangle with the position of spectral colours shown (after Rose).

The spectral sensitivities of the each receptor class (UV, B and G) varies across the surface of the eye surface and in general a single set of functions has not be defined. Menzel has published [MB76] some measured functions for a number of sample sites on the eye and we show representative curves in Figure 6.

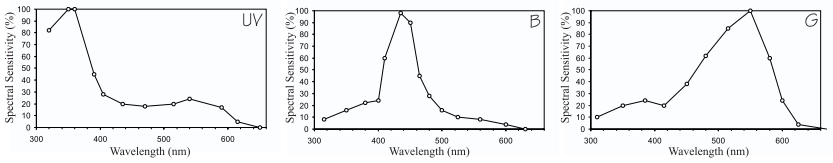

Fig. 6. Spectral sensitivies (from Menzel) of the 3 receptor classes of *Apis meliferra*. (a) $S_{UV}(\lambda)$, (b)$S_B(\lambda)$, (c)$S_G(\lambda)$.

We use these to define a trichromatic colour space by projection of the incident spectral irradiance function, Φ_{in} onto the receptor sensitivites to yield a trichromatic stimulus response tuple (UV, B, G) and integration:

$$UV = \int_{300nm}^{680nm} S_{UV}(\lambda)\Phi_{in}(\lambda)d\lambda \tag{1}$$

$$B = \int_{300nm}^{680nm} S_B(\lambda)\Phi_{in}(\lambda)d\lambda \quad (2)$$

$$G = \int_{300nm}^{680nm} S_G(\lambda)\Phi_{in}(\lambda)d\lambda \quad (3)$$

$$(4)$$

As a visualisation stage, we are then free to apply a number of mappings to facilitate viewing this colour space on an RGB display device. Note that the response scalars and indeed the perceived brightness (inner product of Φ_{in} and S, the overall spectral sensitivity of Figure 5(a)) may not be expressed in terms of normal photometric quantites and are relative stimulus values which may be arbitrarily mapped to display luminance.

4 Implementation

A bidirectional monte-carlo raytracing simulation [Col96] provides estimates of incoming radiance at the receptor. Full spectral sampling is carried out at a user specified sampling density (all results here have used 8 uniformly distributed samples). Each queried ray direction returns a full spectral radiance function ($W/m^2/sr^{-1}/nm$).

4.1 Ommatidia Distribution

In order to generate the bee-eye rays we chose to generate a series of sample points on the surface of the compound eye *a-priori* as the number of sample points is fixed by the number of receptors. The current implementation assumes a worker class bee, although it would be a simple matter to include data for all other classes. Given the receptor distribution shown in Figure 2(a) a matching distribution of points is required over the surface. A 3-stage process is used:

1. A polygonal model matching the geometry of the compound eye was created by hand (see Figure 2(b)) using a modelling tool.
2. A regular grid (see Figure 7(a)) is superimposed over the surface, the resolution of which is chosen to generate approximately the correct number of sample points. Grid vertices projected parallel to the mesh z-axis become initial positions for sample points.
3. The sample points become nodes in a spring-mass particle system, with rest length between mass points determined by the required facet diameter of the associated receptor. Particles are free to move over the surface of the mesh but are prevented from leaving the polygonal mesh. The particle system is iterated until stable within a given tolerance. The final resting positions of the particles are recorded as receptor centers with receptor axis determined from the interpolated normal of the polygon containing the particle.

Note that this process, though expensive, need only be computed once for a given eye geometry and is general enough to facilitate many different geometries. Figure 7(c) shows a number of steps in the particle system evolution. Notice how the particle density increases according to the facet diameter map of Figure 2.

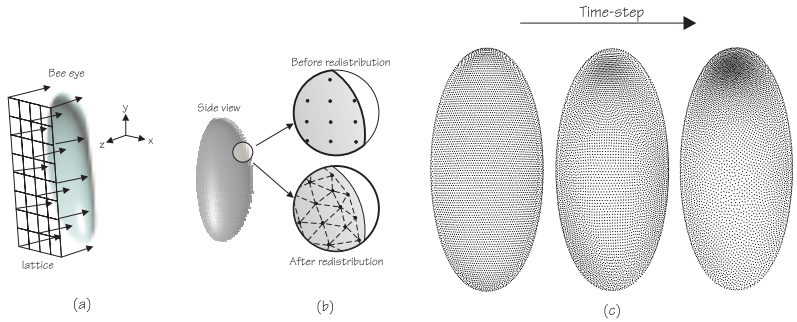

Fig. 7. The sample generation process. Each sample is associated with a single receptor and must define a sample position on the eye surface and receptor axis direction. (a) Samples are distributed uniformly over the eye surface, (b) a spring-mass particle system is used to adaptively reposition samples according to required receptor diameters. (c) depicts three stages in the particle system evolution, with an early stage on the left and a near-final stage on the right.

4.2 Acceptance Function Sampling

To model the acceptance function for individual ommatidia, the solid angle determined by $\Delta\rho$ is *importance sampled* using the Gaussian $A(\theta)$ as an estimator so

$$p(\theta) \propto A(\theta)$$

where $p(\theta)$ is the appropriate probability density function. The total irradiance on the receptor is therefore estimated as

$$\Sigma(\lambda) \approx \frac{1}{n} \sum_{i=1}^{n} \frac{L_{in}(\lambda, \theta_i)}{A(\theta_i)} \text{ where } \theta_i \sim A^{-1}$$

4.3 Image Reconstruction

The result of the simulation is an array of n spectral power curves, one for each receptor. This is a relatively unorganised set of points requiring triangulation or surface fitting for display. It is questionable whether the bee's visual field appears, to the bee, as an array of facets, however we chose to display the image in a manner which highlights this hexagonally faceted nature. This is achieved by creating a *Voronoi diagram* of the points and shading each Voronoi cell according to the perceived colour. Rather that analytically computing and triangulating the Voronoi diagram, a discrete approximation to the diagram is computed by determining the nearest cell to each pixel in the image when the cells are projected parallel to the z-axis of the eye (see Figure 7) onto an image plane. To speed up the process, cells are entered into a 2d *hash table* for efficient nearest neighbour determination. To eliminate edge artifacts, the diagram is clipped by a mask created from the convex hull of the eye geometry.

An alternative approach (as shown in Colour Plate 2) is to employ a density estimation phase to reconstruct the visual field. As can be seen, this is not entirely satisfactory as the luminance of the image varies according to the particle density which is a maximum in the upper left region of the retinal surface.

4.4 Colour Mapping

The mapping of the bee visual characteristic to a gamut suitable for display to a human observer amounts to a visualisation and as such we are free to make a number of choices regarding the nature of this mapping.

We have employed two different colour mapping schemes: the first, **map2**, shown in Colour Plate 3 simply employs the human observer model, but utilises the bee retinal geometry to allow us to comparitively assess the impact of this geometry on the image formed. Note the increase in visual acuity in the upper left region of the image corresponding to the lower facet diameters in this region.

The second, **map3**, shown in Colour Plate 5, generates a trichromatic stimulus tuple (UV, B, G) by projecting the spectral power curve onto S_{UV}, S_B and S_G respectively as detailed in Section 3.2. We can either view these independently (see Colour Plate 4) or map these to the RGB space in some manner. One such possibility is to render the UV channel as red and map the B and G bee channels to the device B and G channels. This has the advantage of producing a white sum on the display when all channels are at unity. Such a mapping is purely arbitrary but should prove useful as a tool for visualisating the data produced from the various studies of the bee's visual system.

Note that in all cases, the sky spectral radiance is predominantly UV and thus shows up most brightly in the UV examples of Colour Plate 4.

5 Results and Conclusions

In producing these initial images we have ignored many aspects of the bee's visual system. In particular we do not address the difficult problems of tone mapping and brightness adaptation, mainly because of the sparsity of data pertaining to these phenomena in the case of the bee.

The particle system approach for generating cellular distributions proves both robust and simple to control, and would easily adapt to the generation of distrubtions for many different retinal types.

Our current test bases are extremely simple and serve only to illustrate the relative responses of the bee's colour channels. To truly aid in visualising bee vision we need to construct models of real-world scenes, with extra information regarding the emitted and reflected UV radiation.

Finally, from a philosophical perspective, it is impossible to accurately represent to a human observer a scene from the point of view of a non-human animal. We can only hope to visualise certain aspects of the visual response.

References

[BM95] Bolin, M.R., Meyer, G.W. A frequency based ray tracer. *Computer Graphics (SIGGRAPH '95 Proceedings)*, pp:409-418.

[Col96] Collins, S., Wavefront Tracking for Global Illumination Solutions, Ph.D. Thesis, Trinity College Dublin, 1996.

[CPC84] Cook, R.L., Porter, T., Carpenter, L. Distributed ray tracing. *Computer Graphics (SIGGRAPH '84 Proceedings)*, vol.18:137-145, July 1984.

[FPSG96] Ferweda, J.A., Pattanaik, S.N., Shirley, P., Greenberg, D.P. A model of visual adaptation for realistic image synthesis. *Computer Graphics (SIGGRAPH '96 Proceedings)*, pp:249-258, 1996.

[Fri67] von Frisch, K. *The dance language and orientation of bees.* Harvard University Press, Cambridge, 1967.

[Gri75] Gribakin, F.G. Functional morphology of the compound eye of the bee. In Horridge, G.A. Ed., *The Compound Eye and Vision of Insects*, pp:154:176, Clarendon Press, Oxford, 1975.

[Hel92] von Helversen, O. Zur spektralen Unterschiedempfindlichkeit der Honigebiene. *J. Comp. Physiol.*, 80:439-472, 1992.

[KMH95] Kolb, C., Mitchell D., Hanrahan, P. A realistic camera model for computer graphics. *Computer Graphics (SIGGRAPH '95 Proceedings)*, pp:317-324, August 1995.

[Lan90] Land, M.F. The design of compound eyes. In Blakemore, C. Ed. *Vision: coding and efficiency*, pp:55-64, Cambridge University Press, Cambridge, 1990.

[MB76] Menzel, R., Blakers, M. Colour receptors in the bee eye - morphology and spectral sensitivity, *J. Comp. Physiol.*, 108:11-33, 1976.

[Mey88] Meyer, G.W. Wavelength selection for synthetic image generation. *Computer Vision, Graphics and Image Processing*, vol.41:57-79, 1988.

[MG88] Meyer, G.W., Greenberg, D.P., Color Defective Vision and Computer Graphics Displays, *IEEE Computer Graphics and Applications*, 8(5):28-40, September 1988.

[NKON90] Eihachiro Nakamae, Kazufumi Kaneda, Takashi Okamoto, Tomoyuki Nishita, A Lighting Model Aiming at Drive Simulators, *Computer Graphics (SIGGRAPH '90 Proceedings)*, (24):395-404, August 1990.

[PC81] Potmesil, M. Chakravarty, I. A lens and aperture model for synthetic image generation. *Computer Graphics (SIGGRAPH '81 Proceedings)*, 15(3):297-305, August 1981.

[PRWW80] van Praagh, J.P., Ribi, W., Wehrhahn, C., Wittmanm, D. Drone bees fixate the queen with the dorsal frontal part of their compound eyes. *J. Comp. Physiol.*, 136:263-266, 1980.

[RM80] Rose, R., Menzel, R. Luminance dependence of pigment color discrimination in bees, *J. Comp. Physiol*, 141:379-388, 1981.

[Sny76] Snyder, A.W. Acuity of compound eyes: physical limitation and design. *J. Comp. Physiol.*, 116:161-182, 1977.

[SSZG95] Spencer, G., Shirley, P., Zimmerman, K., Greenberg, D.P. Physically based glare effects for digital images. *Computer Graphics (SIGGRAPH '95 Proceedings)*, pp:325-334, August 1995.

[TR93] Tumblin, J., Rushmeier, H. Tone reproduction for realistic images, *IEEE Computer Graphics and Applications*, 13(6):42-48.

[War94] Ward, G. A contrast-based scalefactor for luminance display. In P.S. Heckbert (Ed.), *Graphics Gems IV*, Academic Press Professional, Boston.

[Weh75] Wehner, R. Pattern recognition. In Horridge, G.A. Ed., *The Compound Eye and Vision of Insects*, pp:154:176, Clarendon Press, Oxford, 1975.